Biochemistry (Moscow), Vol. 68, No. 5, 2003, pp. 541-550. Translated from Biokhimiya, Vol. 68, No. 5, 2003, pp. 664-675.

Femtosecond Nuclear Oscillations under Charge Separation in Reaction Centers of Photosynthesis

A. G. Yakovlev[1], A. Ya. Shkuropatov[2], and V. A. Shuvalov[1,2]*

[1]*Department of Photobiophysics, Belozersky Institute of Physico-Chemical Biology, Lomonosov Moscow State University, Moscow 119992, Russia; fax: (095) 939-3181; E-mail: yakov@genebee.msu.su*
[2]*Institute of Basic Biological Problems, Russian Academy of Sciences, Pushchino, Moscow Region 142292, Russia; fax: (277) 90532; E-mail: shuvalov@issp.serpukhov.su*

Received April 10, 2002
Revision received May 29, 2002

Abstract—Results are presented of a study of primary processes of formation of the charge separated states $P^+B_A^-$ and $P^+H_A^-$ (where P is the primary electron donor, B_A and H_A the primary and secondary electron acceptors) in native and pheophytin-modified reaction centers (RCs) of *Rhodobacter sphaeroides* R-26 by methods of femtosecond spectroscopy of absorption changes at low temperature. Coherent oscillations were studied in the kinetics at 935 nm (P* stimulated emission band), at 1020 nm (B_A^- absorption band), and at 760 nm (H_A absorption band). It was found that when the wavepacket created under femtosecond light excitation approaches the intersection between P* and $P^+B_A^-$ potential surfaces at 120- and 380-fsec delays, the formation of two electron states emitting light at 935 nm (P*) and absorbing light at 1020 nm ($P^+B_A^-$) takes place. At the later time the wavepacket motion has a frequency of 32 cm^{-1} and is accompanied by electron transfer from P* to B_A in pheophytin-modified and native RCs and further to H_A in native RCs. It was shown that electron transfer processes monitored by the 1020-nm absorption band development as well as by bleaching of 760-nm absorption band have the enhanced 32 cm^{-1} mode in the Fourier transform spectra.

Key words: photosynthesis, reaction center, electron transfer, wavepacket, femtosecond spectroscopy

The reaction center (RC) of purple bacteria consists of three protein subunits (L, M, and H), four bacteriochlorophyll molecules, two bacteriopheophytin molecules, two quinone molecules, and one atom of non-heme iron. The three-dimensional structure of RC was established by X-ray analysis [1-4]. The primary act of charge separation in RC occurs between the excited primary electron donor, P*, bacteriochlorophyll dimer, and a monomeric bacteriochlorophyll B_A forming an intermediate state $P^+B_A^-$ within ~3 psec at 293 K (where A denotes the photoactive branch of the cofactors) [5-13]. Then an electron is transferred from B_A^- to bacteriopheophytin H_A within ~1 psec and from H_A^- to quinone Q_A within ~200 psec. Each of these processes is accelerated by 2-3 times when temperature is decreased to 5-10 K. The formation of P* is accompanied by the bleaching of P absorption bands at 870 and 600 nm and by the appearance of a stimulated emission around 920 nm. The stimulated emission disappears when an electron is transferred from P* to B_A and concomitantly the bleaching of the absorption band of B_A at 800 nm and the development of the absorption band of B_A^- at 1020 nm take place. The formation of $P^+B_A^-$ is difficult to measure in native RCs due to ultrafast conversion of the $P^+B_A^-$ state to the lower-lying $P^+H_A^-$ state but it is observed distinctly in modified RCs in which H_A is replaced by plant pheophytin *a* (Pheo) [10-16]. Since the $Pheo^-$/Pheo redox potential has a more negative value than that for H_A, the free energy level of P^+Pheo^- becomes higher than that of $P^+B_A^-$ by ~200 cm^{-1} [17]. Consequently, the electron transfer in pheophytin-modified RCs from B_A^- to Pheo is delayed significantly. Pheo takes part virtually in the electron transfer from B_A^- to Q_A [17] with a time constant of 1.8 nsec instead of 70 psec observed in native RCs at 5 K [12]. The replacement of H_A by Pheo was found to make no changes in the electron transfer from P* to B_A [12]. As revealed by recombination fluorescence measurements [18, 19], the free energy level of $P^+B_A^-$ is below that of P^*B_A by 350-550 cm^{-1}. The $P^+B_A^-$ recombination time is about 1 nsec [12], which is 3 times slower than the lifetime of P*B (~300 psec).

Abbreviations: ΔA) absorption difference (light minus dark); B_A and H_A) monomer bacteriochlorophyll and bacteriopheophytin in the active chain, respectively; P) bacteriochlorophyll dimer; Pheo) plant pheophytin; Q_A) quinone; RC) reaction center.

* To whom correspondence should be addressed.

0006-2979/03/6805-0541$25.00 ©2003 MAIK "Nauka/Interperiodica"

According to current knowledge, the electron transfer between P* and B_A should occur at the intersection of potential energy surfaces for the P^*B_A and $P^+B_A^-$ states. An effective approach for study of the electron transfer events at the intersection is the measurements of fsec oscillations in the B_A^- product absorption band at 1020 nm (see, for example, [13-16]) which are observed under excitation of P by light pulses of fsec (≤30 fsec) duration and broad spectral width. Under these conditions a nuclear wavepacket is created on the P^*B_A potential energy surface [20, 21]. This wavepacket is a superposition of wavefunctions of several ($2\upsilon + 1$, $\upsilon = 0, 1, 2, ...$) vibrational levels and has properties of a quasi-classical particle [22]:

$$\Psi(x,t) = (2\upsilon + 1)^{-0.5} \sum^j \varphi_{n+j} \exp\{-i\omega(n + j + 0.5)t\}. \quad (1)$$

Here $\Psi(x,t)$ is a wavefunction, x a coordinate, φ_{n+j} a fundamental function of harmonic oscillator, and ω a mechanical oscillation frequency. For a gravity center $\langle x \rangle$ of the wavepacket we have clear time dependence [22]:

$$\langle x \rangle = \int \Psi^*(x,t)\, x\, \Psi(x,t) = A \cos(\omega t). \quad (2)$$

This means that $\langle x \rangle$ changes in time according to a classical equation of harmonic oscillator motion:

$$\langle \ddot{x} \rangle + \omega^2 \langle x \rangle = 0. \quad (3)$$

The motion of the wavepacket on the potential surface is accompanied by emission. The wavepacket emission wavelength depends on time since the nuclear coordinates of the P* and P surfaces are shifted from each other [20, 21]. There are two maxima in the wavepacket emission at 895 and 935 nm, and the oscillations at these maxima have opposite phases [20, 21]. The Fourier transform spectrum of fsec oscillations in stimulated emission of P* at 10 K consists of frequencies at 15, 30, 69, 92, 122, 153, 191, and 329 cm^{-1} [21]. Similar vibrational modes were found at 27, 73, 110, 147, 175, and 205 cm^{-1} in experiments of photochemical hole burning [23]. Resonance Raman scattering experiments also gave the similar frequencies at 34, 71, 95, and 128 cm^{-1} [24].

In [25] results are shown of study of fsec oscillations on *Rh. sphaeroides* RCs in the 920-1100 nm range. The use of too long 100-fsec pulses did not allow discerning the oscillations completely according to [21]. As a result, the authors failed to make a conclusion about the presence of different processes of electron transfer in the measured absorbance changes. But spectral features near 1020 nm in [25] can be interpreted as being a result of addition of out of phase oscillations of the P* stimulated emission band and the B_A^- absorption band.

In works [13-15] we studied the coherent nuclear oscillations in pheophytin-modified RCs of *Rhodobacter sphaeroides* R-26 at room temperature. It was found that in the 1020-nm absorption band oscillations with 130 and 320 cm^{-1} frequencies corresponded to mostly reversible appearance of the $P^+B_A^-$ state, while oscillations with 9 and 32 cm^{-1} frequencies corresponded to irreversible accumulation of this state. In [16] we studied the coherent nuclear oscillations in different states of native RCs of *Rhodobacter sphaeroides* R-26 at room temperature. It was found that there is an intensive oscillation mode at 32 cm^{-1} in the H_A bleaching band at 760 nm as well as in the B_A^- absorption band at 1020 nm. A hypothesis is discussed about wavepacket transmission from the 130-140 cm^{-1} mode surface to the 32 cm^{-1} mode surface.

In the present work, the results of study of fsec nuclear oscillations in native and pheophytin-modified RCs of *Rhodobacter sphaeroides* R-26 at low (90 K) temperature are presented. Quasi-equidistant modes separated by 32 cm^{-1} were founded in the 130-cm^{-1} oscillation band of the product $P^+B_A^-$ at 1020 nm similar to those of P*. It was found that oscillation with a frequency of 32 cm^{-1} dominates in the H_A bleaching band of native RCs at 760 nm. These results were systematically compared with those obtained earlier at room temperature. The probable formation of a mixed state consisting of the P* and $P^+B_A^-$ states on the P* hypersurface including different modes of nuclear oscillations is discussed. Analysis of these results allows drawing a scheme of intersection of potential energy surfaces for different states and throws light on the mechanism of primary processes of charge separation.

MATERIALS AND METHODS

RCs of *Rhodobacter sphaeroides* R-26 were isolated as described in [26] and were pheophytin-modified as described in [11]. The samples were mixed with glycerol (60%) to obtain a transparent ice on freezing. The optical density of the samples was 0.4 at 870 nm at 90 K in the 2-mm cuvette. Sodium dithionite (5 mM) was added to keep the state $PB_AH_AQ_A^-$ in RCs. All measurements were carried out at 90 K.

Measurements of difference (light-minus-dark) absorption spectra with femtosecond resolution were carried out with a home-built laser spectrometer based on Ti:sapphire laser with amplifier, continuum generator, and optical multichannel analyzer described in detail in [13-16]. The operating frequency was 15 Hz. The duration of the pump and probe pulses was about 25 fsec. Pump pulses were centered at 870 nm. The pump and probe pulses had weak (~20%) mutual perpendicular polarization while the remaining part (~80%) was depolarized. The delay between pump and probe pulses was changed with an accuracy of ~10 fsec. The compensation of temporal dispersion in the range from 600 to 900 nm was monitored by kinetic measurements at 600 nm (Q_x transition of P) and at 900 nm (Q_y transition of P and

short wavelength side of stimulated emission from P*). In this range the dispersion was less than 50 fsec. In the 900-935 nm range the dispersion was less than 10 fsec which was checked by out of phase oscillations at 900 and 935 nm according to [20, 21]. In the 930-1040 nm range the dispersion was less than 30 fsec which was checked by in phase oscillations at 935 and 1020 nm according to [13-16]. The same dispersion value of less than 30 fsec was obtained by measurements of absorption band bleaching of the green filter (ZS-10) in the range of 935-1060 nm showed an absence of shape distortions of the bleaching band.

The amplitude of the spectral bands at 935, 1020, and 760 nm at different delays superimposed on the broad background was measured at their maxima as shown by arrows in Fig. 1. The resulting difference (light-minus-dark) absorption spectra were obtained by averaging of 3000-7000 measurements at each delay. The accuracy of spectral measurements was $(1\text{-}2)\cdot10^{-4}$ units of optical density. The kinetics of absorbance changes (ΔA) at different wavelengths were revealed from the difference absorption spectra measured at different delays. Then non-oscillating fits were subtracted from the kinetics and the residual oscillatory parts of the kinetics were Fourier transformed to obtain the spectra of oscillations. The fits were optimized by minimal amplitude of the oscillations.

RESULTS

It is known that femtosecond oscillations in stimulated emission from the primary electron donor excited state P* are caused by the coherent nuclear motion within one electronic state of P* [16, 20, 21, 27, 28]. This is not the case for fsec oscillations observed in the charge transfer states $P^+B_A^-$ and $P^+H_A^-$. Figure 1 (a and b) shows the absorption difference spectra of the 1020-nm band formation (B_A^- band [7, 12]) at different delays in native and pheophytin-modified *Rb. sphaeroides* R-26 RCs at 90 K. Changes in the band shape and maximum position for a whole period of the measurements (0-4 psec) are absent. This means that fsec oscillations observed in the kinetics of the 1020-nm band development (see Figs. 3 and 5) are related to coherent motions between different electronic states (most probably, P* and $P^+B_A^-$) rather than to oscillations within only the product $P^+B_A^-$ state. Figure 1c shows the difference absorption spectra of the H_A band around 760 nm at different delays for native RCs at 90 K. Again the invariability of the band shape and maximum position of this band in the whole range of delays shows that the observed fsec oscillations (see Fig. 6) are caused by coherent nuclear motions between different electronic states (probably $P^+H_A^-$ and $P^+B_A^-$). The same is true at room temperature [16], when the width of the mentioned bands is increased by ~1.5 times.

The double arrows in Fig. 1 demonstrate the approach we used to measure the amplitudes of the 1020-nm band development (B_A^- formation) and the 760-nm band bleaching (H_A^- formation) superimposed on the broad background. This approach permits to find the changes in these bands on the background of other bands (such as P* stimulated emission band, P absorption band, and others). The obtained band amplitudes were employed to plot the kinetics of the different processes. The same was done for the 935-nm band reflecting the P* stimulated emission (see [13, 14]).

Let us to examine the results on pheophytin-modified RCs. Figures 2a and 3a show that the decay of the P* stimulated emission at 935 nm (Fig. 2) and the development of the B_A^- at 1020 nm (Fig. 3) occur at 90 K (solid lines) within ~1.5 psec in agreement with [12] (~3 psec at room temperature (dashed lines)). Superimposed on the non-oscillating quasi-exponential part of the kinetics, fsec oscillations are observed in both processes (Figs. 2b and 3b). Fourier transform spectra of the oscillating components of the kinetics are presented in Figs. 2c and 3c. At 293 K (dashed lines) the 32-cm^{-1} mode dominates in the oscillations of the 1020-nm kinetics (Fig. 3c), while a broad band centered at 125-130 cm^{-1} dominates in the oscillations of the 935-nm kinetics. The main picture is the same in the measurements at 90 K (solid lines). The overtones of the 32 cm^{-1} mode at 65-66, 93-94, 125-126, 158, 187-188, and 222-224 cm^{-1} (calculated as 64, 96, 128, 160, 192, and 224 cm^{-1}) are clearly seen in the Fourier transform spectra at 90 K. The overtones are more intense in the Fourier spectra of P* stimulated emission oscillations at 935 nm. Very similar overtone frequencies were found earlier in oscillations of P* stimulated emission at 10 K [21]. At 293 K the overtones are almost completely absent. The appearance of the higher harmonics (up to the 6th) in the P* stimulated emission oscillation is not characteristic of vibrational modes. One can suppose that these oscillations are related to a rotation of small molecules like OH^- or H_2O connected by a weak hydrogen bond to the photochemically active chromophores.

Now let us to examine the results obtained for native RCs. The kinetics of P* stimulated emission at 935 nm in native RCs (Fig. 4a) are very similar to those in pheophytin-modified RCs. In spite of the presence of efficient electron transfer to H_A the oscillations are present (Fig. 4b) and superimposed on the exponential decay with a characteristic time ~1.5 psec at 90 K (solid lines) and ~3 psec at 293 K (dashed lines) in these kinetics. This suggests that the interactions between P and B_A are similar in native and pheophytin-modified RCs. Fourier spectra frequencies of oscillations at 67, 93, 125, 164, and 194 cm^{-1} of the 935-nm band in native RCs (Fig. 4c) are very similar to those in pheophytin-modified RCs (Fig. 2c) and can also be assigned to the overtones of the 32 cm^{-1} mode.

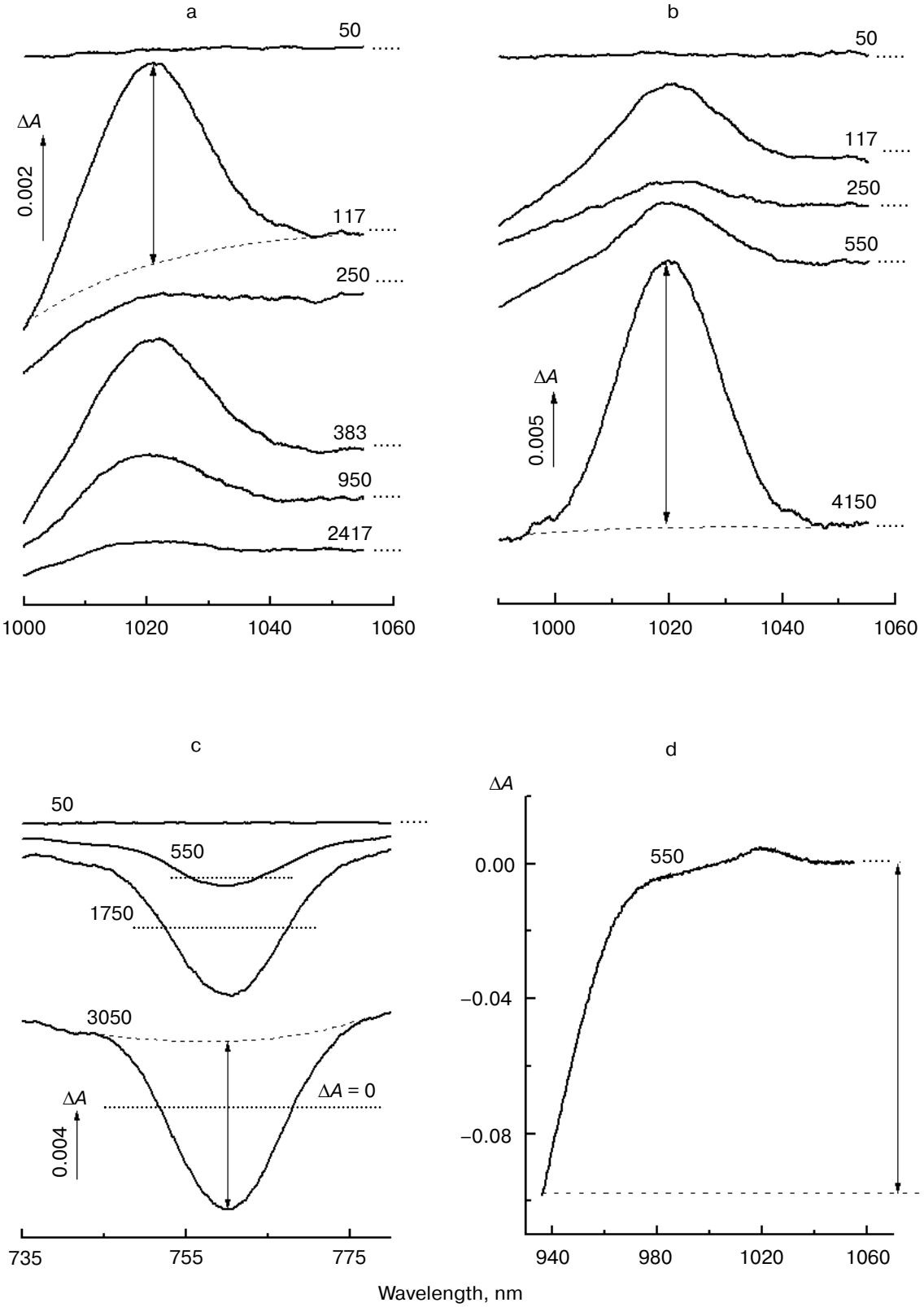

Fig. 1. Difference (light-minus-dark) absorbance spectra at various fsec delays in native (a, c) and pheophytin-modified (b, d) RCs of *Rb. sphaeroides* R-26 excited at 90 K by 25-fsec pulses at 870 nm. a, b) 990-1060 nm range (B_A^- absorption band); c) 735-776 nm range (bleaching of H_A band); d) 935-1060 nm range. Double arrows show the amplitude of absorbance changes (ΔA) of spectral bands at 1020 (a, b), 760 (c), and 935 nm (d) that was used for kinetics plots (see Figs. 2-6). Numbers above the curves are delay values in fsec.

Femtosecond oscillations superimposed on the non-oscillating quasi-exponential part of the kinetics are also observed in the B_A^- absorption band at 1020 nm (Fig. 5a). The 1020-nm kinetics for native RCs are significantly different from those for pheophytin-modified RCs. In native RCs a continuous accumulation of the $P^+B_A^-$ state is absent due to very fast electron transfer from B_A^- to H_A [29] (see Fig. 6) in contrast to pheophytin-modified RCs. Instead of this accumulation, one can see very fast initial increase of absorption in the 1020-nm kinetics followed by its decrease. At 90 K (solid lines) the initial increase is within ~100 fsec, while the following decrease is within ~0.8 psec, so the state $P^+B_A^-$ appeared and then almost completely disappeared during the first 2 psec. At 293 K (dashed lines) the mentioned times are increased by a factor of 2-3, and oscillation maxima at ~2- and ~3-psec delays (Fig. 5b) become more pronounced. Note that the oscillation peaks at 120-fsec delay are very similar in native and pheophytin-modified RCs. At 90 K the later oscillation peaks at 380 fsec and 1 psec are significantly decreased and peaks at 2 and 3 psec are very weak for native RCs comparing with pheophytin-modified RCs. Fourier transform spectrum of oscillations in native RCs at 1020 nm (Fig. 5c) includes the intensive 32 cm^{-1} mode and its overtones at 66, 96, 127, 159, 190, and 223 cm^{-1}.

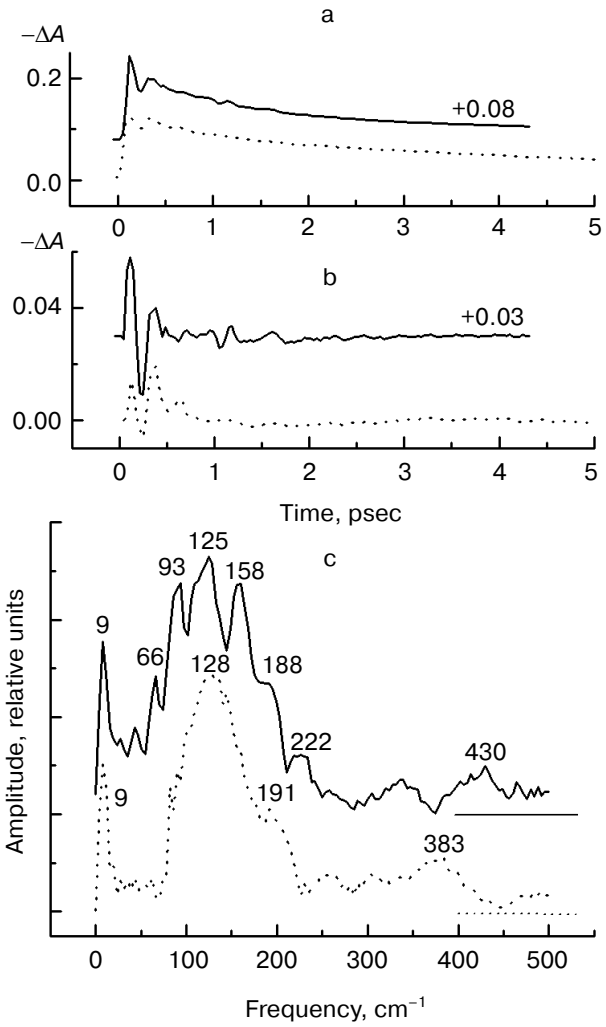

Fig. 2. Kinetics of ΔA (a), its oscillatory part (b), and spectrum of Fourier transform of oscillatory part (c) at 935 nm for pheophytin-modified RCs of *Rb. sphaeroides* R-26 excited by 25-fsec pulses at 870 nm. Solid lines, measurements at 90 K; dashed lines, measurements at 293 K. Numbers in part (c) denote characteristic frequencies of maxima of the Fourier transform spectrum.

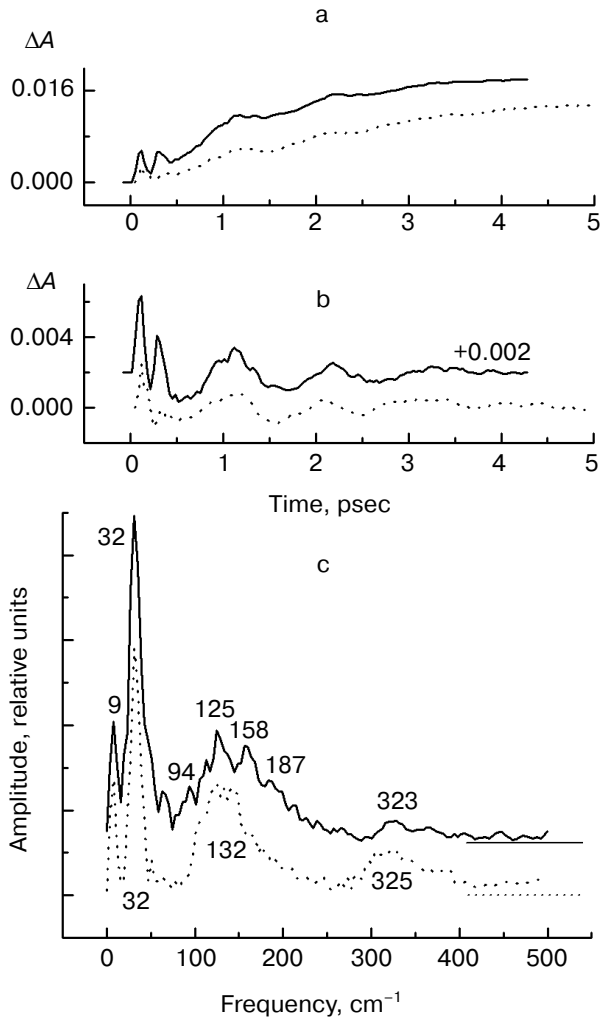

Fig. 3. Kinetics of ΔA (a), its oscillatory part (b), and spectrum of Fourier transform of oscillatory part (c) at 1020 nm for pheophytin-modified RCs of *Rb. sphaeroides* R-26 excited by 25-fsec pulses at 870 nm. Solid lines, measurements at 90 K; dashed lines, measurements at 293 K. Numbers in part (c) denote characteristic frequencies of maxima of the Fourier transform spectrum.

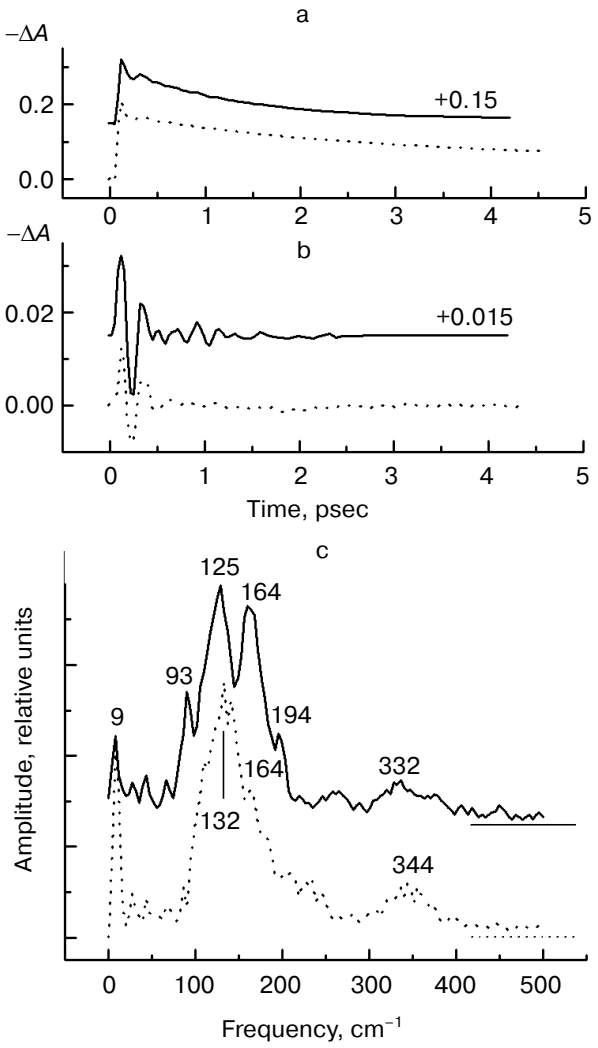

Fig. 4. Kinetics of ΔA (a), its oscillatory part (b), and spectrum of Fourier transform of oscillatory part (c) at 935 nm for native RCs of *Rb. sphaeroides* R-26 excited by 25-fsec pulses at 870 nm. Solid lines, measurements at 90 K; dashed lines, measurements at 293 K. Numbers in part (c) denote characteristic frequencies of maxima of the Fourier transform spectrum.

At 293 K these overtones are significantly less in amplitude (Fig. 5c, dashed line).

The fsec oscillations superimposed on the non-oscillating quasi-exponential part of the kinetics are also observed in the bleaching band at 760 nm reflecting the formation of the H_A^- state in native RCs (Fig. 6). At 90 K the bleaching is almost absent at 120-fsec delay, but then its growth starts with a characteristic time of ~1.5 psec. At 380-fsec and 1.2-psec delays the 760-nm kinetics reflects the appearance of the $P^+H_A^-$ state that is manifested as the integration of the corresponding oscillation peaks of the B_A^- band at 1020 nm over the time (Fig. 6b). This temporal dependence can be explained by the fact that the appearance of the wavepacket on the $P^+B_A^-$ surface leads to effective electron transfer to H_A proportionally to the time of the wavepacket being on the $P^+B_A^-$ surface. At 293 K the electron transfer from B_A^- to H_A is delayed and slowed down (Fig. 6a, dashed line): the appearance of the oscillation peaks at 120 and 380 fsec in the B_A^- band (Fig. 5) is not accompanied by electron transfer from B_A^- to H_A. Only the appearance of the oscillation peaks at ~1, ~2, and ~3 psec in the B_A^- band is accompanied by the electron transfer to H_A with lower efficiency than at 90 K. The Fourier transform spectrum of the oscillations in the 760-nm band at 90 K (Fig. 6c) has a dominant band at 32 cm^{-1} and small bands at 64, 92, and

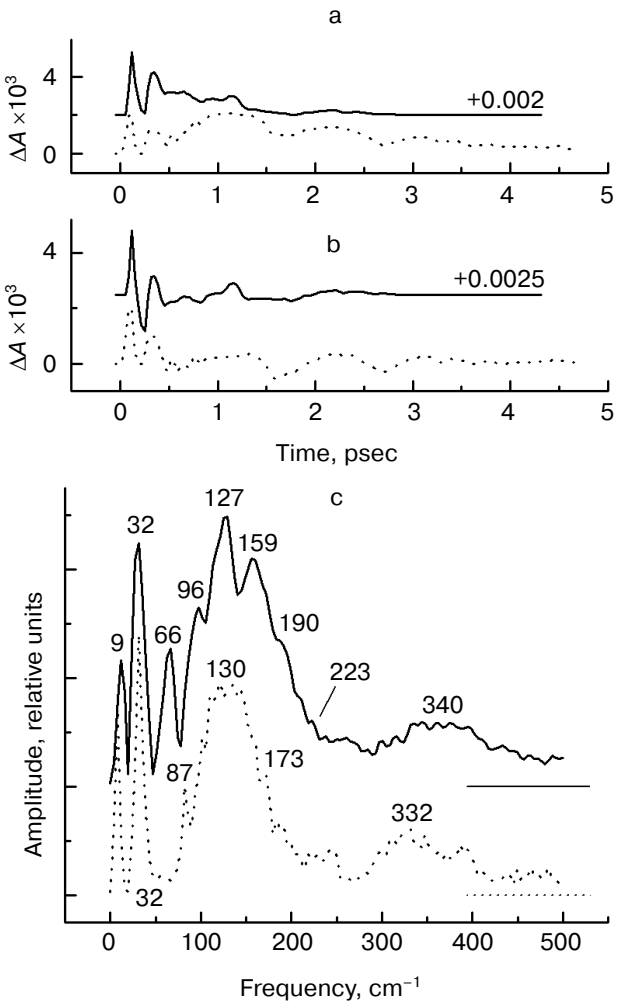

Fig. 5. Kinetics of ΔA (a), its oscillatory part (b) and spectrum of Fourier transform of oscillatory part (c) at 1020 nm for native RCs of *Rb. sphaeroides* R-26 excited by 25-fsec pulses at 870 nm. Solid lines, measurements at 90 K, dashed lines, measurements at 293 K. Numbers in part (c) denote characteristic frequencies of maxima of Fourier transform spectrum.

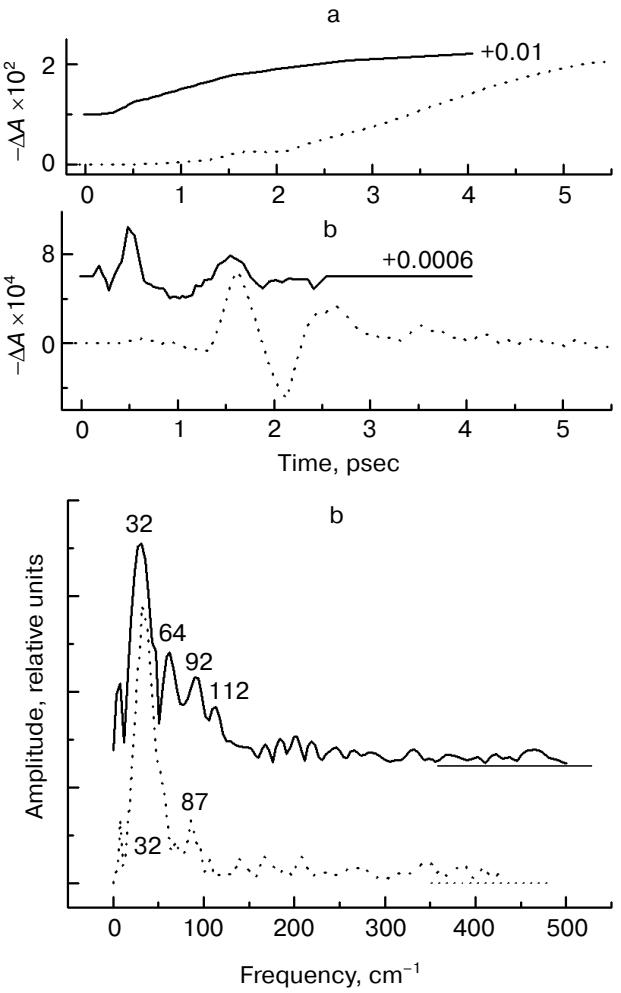

Fig. 6. Kinetics of ΔA (a), its oscillatory part (b), and spectrum of Fourier transform of oscillatory part (c) at 760 nm for native RCs of *Rb. sphaeroides* R-26 excited by 25-fsec pulses at 870 nm. Solid lines, measurements at 90 K; dashed lines, measurements at 293 K. Numbers in part (c) denote characteristic frequencies of maxima of the Fourier transform spectrum.

112 cm^{-1}. It should be noted that the Fourier transform spectrum does not include frequencies around 130 cm^{-1}, which is character for the Fourier spectra of the kinetics at 935 and 1020 nm (Figs. 4c and 5c). This fact suggests that the 130 cm^{-1} mode and the 32 cm^{-1} mode overtones are not active in the wavepacket transfer to the $P^+H_A^-$ potential energy surface.

At 293 K the Fourier transform spectrum of the oscillations at 760 nm include only one band at 32 cm^{-1} (Fig. 6c, dashed line). The 32-cm^{-1} band of the Fourier transform spectrum of the oscillations was found also around 788 nm by direct kinetics measurements (without separation of spectral components of various absorption bands) [30].

DISCUSSION

The described results allow drawing the potential energy scheme for non-equilibrium conversion of the excited state P* into the charge separated states ($P^+B_A^-H_A$ and $P^+B_AH_A^-$) in bacterial reaction centers (Fig. 7). The first step of the conversion was theoretically described in [31] by a harmonic bath model using the diabatic Hamiltonians for the ground (PB_A, $H_1 = K + \Sigma_i \hbar\omega_i(x_i - \xi_i/(\hbar\omega_i))^2/2 + \Sigma_j \hbar\omega_j y_j^2/2 + \varepsilon_1$), locally excited ($P^*B_A$, $H_2 = K + \Sigma_i \hbar\omega_i x_i^2/2 + \Sigma_j \hbar\omega_j y_j^2/2$) and charge transfer ($P^+B_A^-$, $H_3 = K + \Sigma_i \hbar\omega_i(x_i - \xi_i'/(\hbar\omega_i))^2/2 + \Sigma_j \hbar\omega_j (y_j - \eta_j/(\hbar\omega_j))^2/2 + \varepsilon_3$) states. Here K is the kinetic energy; x_i and y_j are the dimensionless coordinates; ε_1 and ε_3 are the energy differences of the potential minima for H_1 and H_3 from H_2, $\hbar$ is Planck constant. The reaction coordinates Q_1 and Q_2 [31] are defined for the photoexcitation and the electron transfer processes, respectively. The angle (θ) between Q_1 ($\equiv\Sigma_i\xi_i x_i$) and Q_2 ($\equiv\Sigma_i\xi_i' x_i + \Sigma_j\eta_j y_j$) determines the amplitude of the fsec oscillation in the electron transfer rate treated by the Landau–Zener semiclassic approach: when $\cos\theta = -1$ (linear arrangement), the oscillations are maximal; when $\cos\theta = 0$ (orthogonal arrangement), the oscillations are absent. The same is true for the average fsec motion of the x-part of the reaction coordinate [31]:

$$Q_{2x}(t) = \Sigma_i \xi_i\xi_i' \cos(\omega_i t)/(\hbar\omega_i). \quad (4)$$

Oscillations of $Q_{2x}(t)$ are maximal when $\cos\theta = -1$ and minimal when $\cos\theta = 0$. The remarkable oscillations in the product $P^+B_A^-$ at 1020 nm indicate that the angle θ is close to 180° (and $\cos\theta \approx -1$). Therefore, one can cut the diabatic potential energy surfaces along Q_1 and Q_2 coordinates. The result of this one-dimension cross-section is shown in Fig. 7.

The transition coefficient k at the crossing place of the P* and $P^+B_A^-$ surfaces can be written as follows:

$$k(\dot{Q}) \equiv P_{LZ}(|\dot{Q}|)\theta(\dot{Q}) + P_{LZ}(|\dot{Q}|)/(1 + P_{LZ}(|\dot{Q}|)). \quad (5)$$

Here $\theta(x)$ is the Heaviside unit function and $P_{LZ}(|\dot{Q}|)$ is the transition probability, for which the following Landau–Zener form is assumed:

$$P_{LZ}(|\dot{Q}|) = 1 - \exp(-2\pi J^2/(\hbar|\dot{Q}|)), \quad (6)$$

where J is the electronic coupling for the electron transfer.

In RCs the wavepacket is initially formed by fsec light pulses on the 130-140 cm^{-1} potential energy surface of P* at the short-wavelength side of the stimulated emission band from P* (895 nm) (Fig. 7). No $P^+B_A^-$ state is observed at this side of the surface. Then the wavepacket begins the motion on the 130-140 cm^{-1} surface towards the long-wavelength side of the stimulated emission band

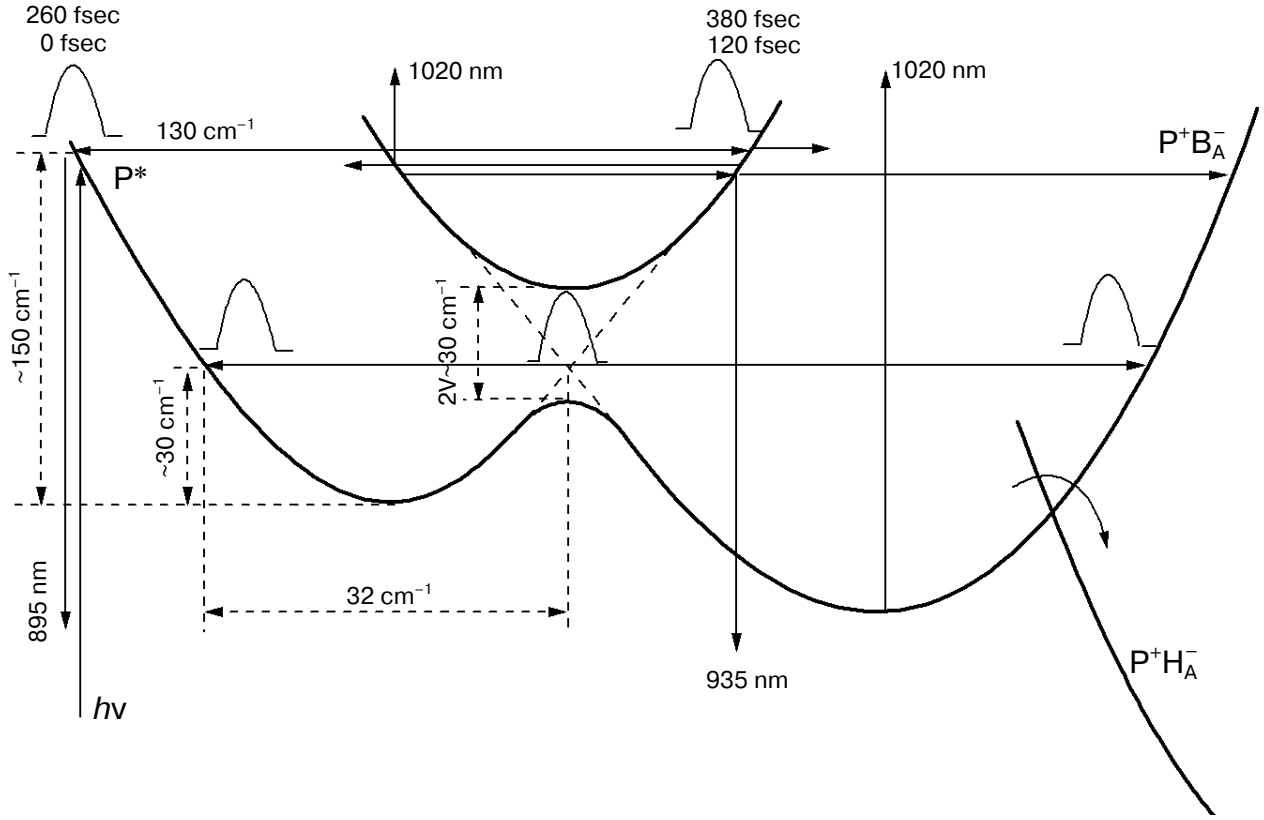

Fig. 7. Schematic representation of the diabatic potential energy surfaces of the locally excited ($P^*B_AH_A$) and charge transfer ($P^+B_A^-H_A$) and ($P^+B_AH_A^-$) states. An electronic coupling between P* and B_A [31] splits two original surfaces (P* and $P^+B_A^-H_A$) into two new surfaces (upper and lower). A high energy (~150 cm^{-1}) wavepacket can approach the upper part of the $P^*B_AH_A$ and $P^+B_A^-H_A$ surfaces intersection and produce emission at 935 nm (P*) and absorption at 1020 nm (B_A^-). The 32 cm^{-1} vibrational mode represents the wavepacket motion on the lower mixing diabatic surface including the P* and $P^+B_A^-H_A$ states. The $P^+B_AH_A^-$ surface is suggested to cross the mixing surface at its part having charge transfer character ($P^+B_A^-H_A$). Another possibility is that the 32 cm^{-1} mode is primary generated on the P* hypersurface from which a low energy wavepacket is transferred to the $P^+B_A^-H_A$ surface at the intersection point.

of P (935 nm). At 120-fsec delay the wavepacket approaches the intersection point between P* and $P^+B_A^-$ surfaces, since the 1020-nm absorption band is formed (Fig. 1).

The estimation of the wavepacket energy gives a value of about 150 cm^{-1} (11,173 cm^{-1} (895 nm), 11,025 cm^{-1} (907 nm as 0–0 transition)) above the bottom of the P* surface. The intersection point is above the bottom by ~30 cm^{-1} [15]. Therefore, at the first (120 fsec) and second (380 fsec) approaches of the wavepacket to the intersection region the wavepacket energy should be above the intersection point by ~120 cm^{-1}. According to [31] in this region the reflections from walls of potential wells of both (P* and $P^+B_A^-$) states are possible. The wavepacket at the P* surface wall emits light at 935 nm and at the $P^+B_A^-$ surface wall absorbs light at 1020 nm. Figures 2 and 3 show that relative amplitudes of the oscillations at 120 fsec delay for the 935-nm (0.19) and 1020-nm (0.20) bands are very similar (see also [13, 14]). This fact might suggest that each wavepacket approaching the long-wavelength side of the stimulated emission at 935 nm approaches the $P^+B_A^-$ surface as well. However, no wavepacket transfer from the P* to $P^+B_A^-$ surface and no electron transfer to H_A is observed at 120 fsec. Figure 1 shows that the 1020-nm band disappears almost completely at longer 250-fsec delay and the 760-nm band does not bleach. This means that all wavepackets at 120 fsec (and most of them at 380 fsec at room temperature) are reflected back to the left side of the P* surface. Only after several reflections and loosing of part of the energy the wavepacket approaches the intersection point at ~30 cm^{-1} above the bottom of the P* surface. Herewith the electronic coupling splits two surfaces into two new surfaces (see Fig. 7). There is the first possibility that the lower surface is formed as a diabatic surface including two states P* and $P^+B_A^-$. This mixing surface has a characteristic frequency of 32 cm^{-1}. The wavepacket motion on this surface is accompanied by an adiabatic electron transfer between two states. The second possibility is related to the formation of the hypersurface of the state

P* which includes both the 130 and 32 cm^{-1} frequency modes. Herewith the motion with the frequency of 32 cm^{-1} leads to the wavepacket transfer to the $P^+B_A^-$ surface. Let us to examine in detail these two possible wavepacket motions on the 32 cm^{-1} surface.

First possibility. Final electron transfer to H_A can be good evidence for the wavepacket appearance on the $P^+B_A^-$ surface. The main frequency component for the $P^+H_A^-$ formation measured at 760 nm is 32 cm^{-1} (Fig. 6c). This frequency can be related to the appearance of the wavepacket on the $P^+B_A^-$ surface, which makes possible the electron transfer to H_A. In fact, the same frequency 32 cm^{-1} is also a main frequency component for the $P^+B_A^-$ formation measured at 1020 nm (Fig. 5c).

The probability of wavepacket transfer directly from the intersection point between the P* and $P^+B_A^-$ surfaces to the $P^+H_A^-$ surface is too small since there is probably no intersection of three surfaces at the same point. This conclusion is supported by the fact that the kinetics of ΔA at 1020 and 760 nm are different, and part of the 760-nm kinetics oscillating with the frequency of 32 cm^{-1} is delayed with respect to those of the 1020-nm band (Figs. 5b and 6b). The simulation of the process shows that the kinetics of the 760-nm band bleaching reflects the integration of the 1020-nm peaks over the time. It is reasonable because the appearance of the wavepacket on the $P^+B_A^-$ surface leads to the electron transfer to H_A proportionally to the time of wavepacket being on the $P^+B_A^-$ surface. We can assume that the 32 cm^{-1} mode includes motions on both the P* and $P^+B_A^-$ surfaces along coordinate Q_2 which allow the electron transfer to H_A when the wavepacket is on the $P^+B_A^-$ part of the 32 cm^{-1} surface (Fig. 7). In other words, the P* and $P^+B_A^-$ states can form a diabatic surface, part of which has charge transfer character of the $P^+B_A^-$ surface. Wavepacket motion between P* and $P^+B_A^-$ might have sufficient probability if this motion causes distance and orientation changes between P and B_A. This was shown in molecular dynamics calculations for two modes at 17 and 28 cm^{-1} [32].

The kinetics for the 1020-nm band has very similar oscillatory parts for both native and Pheo-modified RCs (Figs. 3b and 5b), especially at 293 K. In Pheo-modified RCs the 32-cm^{-1} oscillation observed in the 1020-nm band kinetics can correspond only to the oscillation of the wavepacket between two surfaces of P* and $P^+B_A^-$ because no electron transfer to Pheo is observed in the psec time domain in these RCs. In native RCs this electron transfer is possible and the appearance of the main peaks in the 760-nm band kinetics coincides in time with ends of the 1020-nm band peaks (Figs. 5b and 6b).

Second possibility. The 32-cm^{-1} mode was observed earlier by us for the $P^+B_A^-$ state in Pheo-modified RCs [13-15] and in native RCs at 293 K [16]. It was suggested that this mode is related to the oscillation on the P* surface. However, the 27-cm^{-1} mode is observed in hole-burning experiments [23] and in fsec kinetics of the stimulated emission at 890 nm [33] and 935 nm (Figs. 2 and 4). This mode is different from the 32-cm^{-1} mode in frequency position and shows a peak of relatively small amplitude in the Fourier transform spectra. On the other hand, the frequencies in the Fourier spectrum for the 935- and 1020-nm kinetics (Figs. 2c-5c) at 66, 93-96, 125-127, 158-164, 187-194, and 222-223 cm^{-1} can be interpreted as overtones (calculated as 64, 96, 128, 160, 192, and 224 cm^{-1}) for the fundamental frequency at 32 cm^{-1}. Similar frequencies have earlier been found in fsec kinetic measurements at 10 K [21]. These results can show that the formation of the wavepacket with frequency of 130-140 cm^{-1} on the hypersurface of P* leads to the subsequent population of the 32 cm^{-1} mode and its overtones since the wavepacket energy for the 130-140 cm^{-1} mode is about 5 times larger than that for the 32 cm^{-1} mode. If this is true, the 32 cm^{-1} mode might belong to the P* hypersurface as well. Then the appearance of the wavepacket on the $P^+B_A^-$ surface with a frequency of 32 cm^{-1} is a result of the wavepacket motion on the P* surface and of an effective transmission of the wavepacket to the $P^+B_A^-$ surface with the same frequency. Since the electron transfer from B_A^- to H_A depends on the appearance of the state $P^+B_A^-$ it is reasonable that $P^+H_A^-$ appears with the same frequency of 32 cm^{-1}.

Besides, the 32 cm^{-1} mode can be related to a rotation of small molecules like OH^- or H_2O connected by a hydrogen bond to the photochemically active chromophores. Two molecules of H_2O are known to be bound by hydrogen bonds to His L173 and M202 on one side and to an oxygen group of B_A and B_B on other side [3]. Approximate calculations of characteristic rotation frequencies according to [34] give a frequency of 37.8 cm^{-1} for OH^- and 29.14 cm^{-1} for H_2O that is very close to the experimental frequency of 32 cm^{-1}. Therefore, the observed sequence of almost equidistant peaks in the Fourier transform spectra of oscillations at 935 and 1020 nm at 90 K can be related to modulation of fsec kinetics by the rotation of H_2O (or OH^-). The same is probably true at room temperature. Further studies of the oscillations in different states of RCs will permit a choice of one of the mentioned possibilities.

From the results obtained we suggest that abovementioned modulation is along the reaction coordinate of the primary charge separation $P^* \rightarrow P^+B_A^-$. This modulation can be important for the electron transfer from the neutral P* to B_A. From Fig. 7 it is clear that the wavepackets with the overtone frequencies at 66, 93, 125, 158, 188, and 222 cm^{-1} are higher in energy than the intersection point between the P* and $P^+B_A^-$ surfaces. Therefore these harmonics appear in the stimulated emission from P* at 935 nm rather than in the 1020 nm kinetics. Small amplitudes of those harmonics observed in the 1020-nm kinetics are probably due to some reflections in the surface region above the intersection point. On the other hand, the wavepacket with the frequency of 32 cm^{-1} and small

energy about 30 cm^{-1} is probably able to penetrate through the split region between the P* and $P^+B_A^-$ surfaces. This leads to the formation of $P^+B_A^-$ state at delays of ~1, ~2, and ~3 psec with the frequency of 32 cm^{-1}. The formation of the state $P^+B_A^-$ causes the electron transfer to H_A in native RCs both at low and at room temperatures with the same 32 cm^{-1} frequency. At low temperature (90 K) the distinct electron transfer from B_A^- to H_A starts already at 380-fsec delay that is much earlier than at 293 K (Fig. 6b). This means that at 90 K the transmission of the wavepacket from the P* to $P^+B_A^-$ surface is increased at 380 fsec with respect to those at room temperature.

The authors thank Dr. A. V. Sharkov for technical help and V. A. Shkuropatova for preparing the samples. This work was partly supported by the Russian Foundation for Basic Research (grant No. 02-04-48650), and an NWO (The Netherlands) grant.

REFERENCES

1. Deisenhofer, J., Epp, O., Miki, K., Huber, R., and Michel, H. (1984) *Mol. Biol.*, **180**, 385-398.
2. Deisenhofer, J., Epp, O., Miki, K., Huber, R., and Michel, H. (1985) *Nature*, **318**, 618-624.
3. Michel, H., Epp, O., and Deisenhofer, J. (1986) *EMBO J.*, **5**, 2445-2451.
4. Komiya, H., Yeates, T. O., Rees, D. C., Allen, J. P., and Feher, G. (1988) *Proc. Natl. Acad. Sci. USA*, **85**, 9012-9016.
5. Shuvalov, V. A., Klevanik, A. V., Sharkov, A. V., Matveetz, Yu. A., and Krukov, P. G. (1978) *FEBS Lett.*, **91**, 135-139.
6. Shuvalov, V. A., and Duysens, L. N. M. (1986) *Proc. Natl. Acad. Sci. USA*, **83**, 1690-1694.
7. Arlt, T., Schmidt, S., Kaiser, W., Lanterwasser, C., Meyer, M., Scheer, H., and Zinth, W. (1993) *Proc. Natl. Acad. Sci. USA*, **90**, 11757-11761.
8. Chekalin, S. V., Matveetz, Yu. A., Shkuropatov, A. Ya., Shuvalov, V. A., and Yartzev, A. P. (1987) *FEBS Lett.*, **216**, 245-248.
9. Schmidt, S., Arlt, T., Hamm, P., Huber, H., Nagele, T., Wachtveitl, J., Meyer, M., Scheer, H., and Zinth, W. (1994) *Chem. Phys. Lett.*, **223**, 116-120.
10. Schmidt, S., Arlt, T., Hamm, P., Huber, H., Nagele, T., Wachtveitl, J., Zinth, W., Meyer, M., and Scheer, H. (1995) *Spectrochim. Acta, Pt. A*, **51**, 1565-1578.
11. Shkuropatov, A. Ya., and Shuvalov, V. A. (1993) *FEBS Lett.*, **322**, 168-172.
12. Kennis, J. T. M., Shkuropatov, A. Ya., van Stokkum, I. H. M., Gast, P., Hoff, A. J., Shuvalov, V. A., and Aartsma, T. J. (1997) *Biochemistry*, **36**, 16231-16238.
13. Yakovlev, A. G., and Shuvalov, V. A. (2000) *J. Chin. Chem. Soc.*, **47**, 709-714.
14. Yakovlev, A. G., Shkuropatov, A. Ya., and Shuvalov, V. A. (2000) *FEBS Lett.*, **466**, 209-212.
15. Yakovlev, A. G., and Shuvalov, V. A. (2001) *Biochemistry (Moscow)*, **66**, 211-220.
16. Yakovlev, A. G., Shkuropatov, A. Ya., and Shuvalov, V. A. (2002) *Biochemistry*, **41**, 2667-2674.
17. Franken, E. M., Shkuropatov, A. Ya., Franke, C., Neerken, S., Gast, P., Shuvalov V. A., Hoff, A. J., and Aartsma, T. J. (1997) *Biochim. Biophys. Acta*, **1321**, 1-9.
18. Shuvalov, V. A., and Yakovlev, A. G. (1998) *Membr. Cell Biol.*, **12**, 563-569.
19. Nowak, F. R., Kennis, J. T. M., Franken, E. M., Shkuropatov, A. Ya., Yakovlev, A. G., Gast, P., Hoff, A. J., Aartsma, T. J., and Shuvalov, V. A. (1998) *Proc. XI Int. Congr. on Photosynthesis*, Kluwer Academic Publishers, Dordrecht, pp. 783-786.
20. Vos, M., Rappaport, F., Lambry, J.-C., Breton, J., and Martin, J.-L. (1993) *Nature*, **363**, 320-325.
21. Vos, M., Jones, M. R., Hunter, C. N., Breton, J., Lambry, J.-C., and Martin, J.-L. (1994) *Biochemistry*, **33**, 6750-6757.
22. Sokolov, A. A., Loskutov, Yu. M., and Ternov, I. M. (1962) *Quantum Mechanics* [in Russian], Uchpedgiz, Moscow.
23. Shuvalov, V. A., Klevanik, A. V., Ganago, A. O., Shkuropatov, A. Ya., and Gubanov, V. S. (1988) *FEBS Lett.*, **237**, 57-60.
24. Cherepy, N. J., Shreve, A. P., Moore, L. J., Franzen, S., Boxer, S. G., and Mathies, R. A. (1994) *J. Phys. Chem.*, **98**, 6023-6029.
25. Spörlein, S., Zinth, W., and Watchtveitl, J. (1998) *J. Phys. Chem. B*, **102**, 7492-7496.
26. Shuvalov, V. A., Shkuropatov, A. Y., Kulakova, S. M., Ismailov, M. A., and Shkuropatova, V. A. (1986) *Biochim. Biophys. Acta*, **849**, 337-348.
27. Vos, M. H., Jones, M. R., McGlynn, P., Hunter, C. N., Breton, J., and Martin, J.-L. (1994) *Biochim. Biophys. Acta*, **1186**, 117-122.
28. Vos, M. H., Jones, M. R., Hunter, C. N., Breton, J., and Martin, J.-L. (1994) *Proc. Natl. Acad. Sci. USA*, **91**, 12701-12705.
29. Lauterwasser, C., Finkele, U., Scheer, H., and Zinth, W. (1991) *Chem. Phys. Lett.*, **183**, 471-477.
30. Vos, H. M., Rischel, C., Jones, M. R., and Martin, J.-L. (2000) *Biochemistry*, **39**, 8353-8361.
31. Ando, K., and Sumi, H. (1998) *J. Phys. Chem. B*, **102**, 10991-11000.
32. Parson, W. W., Chu, Z. T., and Warshel, A. (1998) *Photosynth. Res.*, **55**, 147-152.
33. Streltsov, A. M., Vulto, S. I. E., Shkuropatov, A. Ya., Hoff, A. J., Aartsma, T. J., and Shuvalov, V. A. (1998) *J. Phys. Chem. B*, **102**, 7293-7298.
34. Herzberg, H. (1949) *Vibrational and Rotational Spectra of Multiatomic Molecules* [Russian translation], Izd-vo Inostr. Literatuty, Moscow.